Automatic Resonance Frequency Tuning Method for Repeater in Resonant Inductive Coupling Wireless Power Transfer Systems

Masataka Ishihara, Kazuhiro Umetani and Eiji Hiraki
Graduate School of Natural Science and Technology
Okayama University
Okayama, Japan

Published in: 2018 International Power Electronics Conference
(IPEC-Niigata 2018 -ECCE Asia)

© 2018 IEEE. Personal use of this material is permitted. Permission from IEEE must be obtained for all other uses, in any current or future media, including reprinting/republishing this material for advertising or promotional purposes, creating new collective works, for resale or redistribution to servers or lists, or reuse of any copyrighted component of this work in other works.

DOI: 10.23919/IPEC.2018.8507768

Automatic Resonance Frequency Tuning Method for Repeater in Resonant Inductive Coupling Wireless Power Transfer Systems

Masataka Ishihara[1*], Kazuhiro Umetani[1] and Eiji Hiraki[1]
1 Graduate School of Natural Science and Technology, Okayama University, Okayama, Japan
*E-mail: p4wv0vf6@s.okayama-u.ac.jp

***Abstract*— Intermediate resonator (repeater) in resonant inductive coupling wireless power transfer (RIC-WPT) systems can increase the transmission distance between the transmitting and receiving coils. The induced current in the repeater is easily affected by the frequency splitting phenomenon because the quality factor (*Q*-factor) of the repeater is generally as high as several hundreds. If this phenomenon occurs, induction of large current is often difficult in the repeater because the one peak characteristic of the induced current is no longer expected and the single peak of resonance splits into multiple peaks which shift the resonant frequency corresponding to the circuit parameters. In this paper, we approach this difficulty by applying an auxiliary circuit to the RIC-WPT system with the repeater. As a result, under the fixed operating frequency, the induced current in the repeater can be kept large even if the frequency splitting phenomenon occurs. The effectiveness of proposed system was supported by the simulation and experiment.**

Keywords*— *wireless power transfer, repeater, automatic tuning, frequency splitting phenomenon

I. INTRODUCTION

Resonant inductive coupling wireless power transfer (RIC-WPT) has recently been actively researched as a high efficiency wireless power transfer technique for various applications such as electric vehicles [1, 2], mobile devices, implanted biomedical devices [3], etc. The RIC-WPT systems utilize the magnetic induction between the magnetically coupled transmitting and receiving coils to transfer the power.

However, the transmission distance between the transmitting and receiving coils is relatively short because the magnitude of the magnetic coupling becomes significantly weak as the transmission distance increases [4, 5]. Therefore, in order to apply RIC-WPT technique to various practical applications, increasing the transmission distance is essential.

As a method of improving the transmission distance, adding the intermediate resonator (repeater) in addition to the transmitting and receiving coils has been widely studied [2, 4–6]. As shown in Fig. 1, the repeater is inserted at an arbitrary place between the transmitting resonator (transmitter) and the receiving resonator (receiver), where W_1–W_3 represent the transmitting, repeating, and receiving coils, respectively.

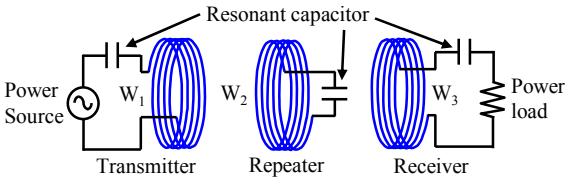

Fig. 1. RIC-WPT system with repeater.

As shown in Fig. 1, because the repeater has a passive configuration with only a coil and a capacitor, the quality factor (*Q*-factor) is as high as about several hundreds. Therefore, the repeater is easily excited by the little main flux generated by the transmitter. As a result, the transmission distance between the transmitter and the receiver can be increased because the repeater can generate the magnetic field by its resonance even in the location far from the transmitter.

However, the repeater tends to have low robustness against the misalignment due to its high *Q*-factor. The reason is that the high *Q*-factor easily leads to the frequency splitting phenomenon [7–12] even under weak magnetic coupling. When the frequency splitting phenomenon occurs, the RIC-WPT system has multiple resonance modes [10]. In other words, the one peak characteristics of the induced current is destroyed and the single peak of resonance splits into multiple peaks with different resonance frequencies. Especially in the RIC-WPT system configured by two coupled resonators, two resonance frequencies appear when the frequency splitting phenomenon occurs [7–12]. Among these two resonance frequencies, the lower frequency corresponds to the odd mode while the higher frequency corresponds to the even mode [8, 10].

The resonance frequencies of these multiple resonance modes are shifted according to the shift of the circuit parameters such as the change in the magnetic coupling factor [8, 11] due to the tolerance of the location of the resonators and the natural tolerance of the inductance or capacitance in the resonators. Therefore, optimum operation is commonly difficult, if the parameters of the

resonator or the operating frequency cannot be adjusted to follow the resonance frequencies. However, if the frequency of the main magnetic flux generated by the transmitter deviates from the resonance frequencies corresponding to the resonance modes, the induced current in the repeater significantly decreases. As a result, the repeater does not operate effectively, causing difficulty in increasing the transmission distance.

There can be two possible approaches to solve this problem: One is dynamical adjustment of the operating frequency [11, 12]; and the other is dynamical adjustment of the resonance frequency of the resonator [9, 13–17], according to the condition of the magnetic coupling.

The former approach can be easily implemented because no additional circuit component is necessary [13]. However, in some case, this approach may not be effective, because the operating frequency may exceed frequency regulation for a RIC-WPT system allowed in a narrow bandwidth [9, 14]. In addition, if multiple resonators in the RIC-WPT system have different resonance frequency due to the manufacturing error, only adjusting the operating frequency is difficult for the practical applications [13]. Therefore, in these cases, the latter approach, i.e. adjusting the resonance frequency of the resonator, may be preferable.

Several methods have been previously proposed as a technique for actively adjusting the resonance frequency [13–17]. Many of these techniques, however, require an additional controller for the adjustment, which may lead to complexity in the circuit implementation. In order to overcome this drawback, [17] has proposed a simple circuit named as the Automatic Tuning Assist Circuit (ATAC), which can adjust the resonance frequency without any controller.

The ATAC is originally proposed to application for the transmitting resonator. According to [17], the ATAC can automatically tune the resonance frequency at the operating frequency. The ATAC can adjust the current phase of the resonator to achieve the unity power factor, which indicates the adjustment of the resonance frequency, only by driving the ATAC in synchronization with the operating frequency.

The previous study [17] has successfully elucidated effectiveness of the ATAC in the transmitting resonator under the one peak characteristic. However, effectiveness of the ATAC in the other resonators or under the frequency splitting phenomenon is still unknown. Particularly, as discussed above, adjustment of the resonance frequency at the repeater, which may easily be operated under the frequency splitting phenomenon, may be important for practical WPT systems. Therefore, the effectiveness of the ATAC should also be investigated in the application to the repeater.

The purpose of this paper is to elucidate the effectiveness of the ATAC for improving the robustness of the performance of the repeater. This paper focuses on the effect of the misalignment of the repeater and elucidates robust power transfer performance regardless to the resultant change in the coupling coefficient. Particularly, this paper verifies the effectiveness of the ATAC for the improvement of the robustness of the repeater when the frequency splitting phenomenon occurs.

The following discussion consists of three sections. Section II reviews the basic operation principle of the ATAC. Section III analyzes the RIC-WPT system with the repeater which applied the ATAC. Section IV presents simulation and experimental results to verify and discuss the effectiveness of the proposed system. Finally, section V presents the conclusions.

II. Operation Principle of ATAC

In this section, the basic operating principle of the ATAC is explained using a circuit shown in Fig. 2 which a single resonator and the ATAC are connected, where r_r is the series parasitic resistance of the resonator, L_r is the self-inductance of the coil, C_r is the resonating capacitance, C_A is the capacitance of the smoothing capacitor, and V_s is the voltage of source.

As shown in Fig. 2, the ATAC consists of the four switches Q_1–Q_4 and a capacitor C_A which has the capacitance sufficiently larger than the resonance capacitor C_r. In some cases, the ATAC having half-bridge configuration which consists of two switches may be used as reported in [17]. Two switches are turned on and off in pair, Q_1 and Q_4 are always opposite to Q_2 and Q_3. Q_1 and

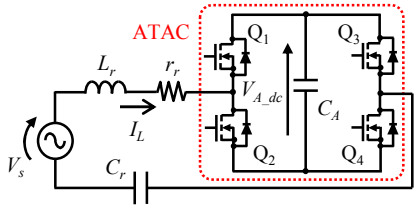

Fig. 2. Single resonator with ATAC.

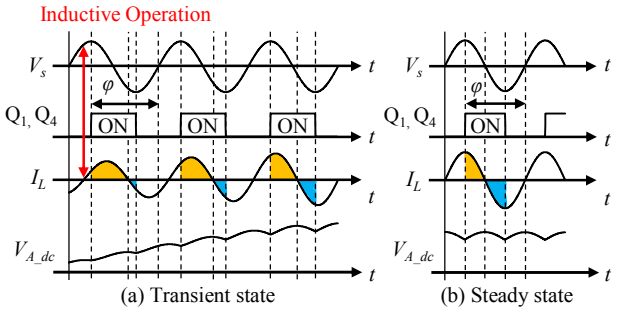

Fig. 3. Operating waveform of Fig. 2 in inductive operation.

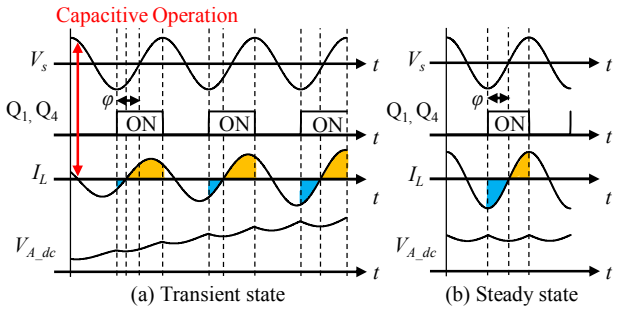

Fig. 4. Operating waveform of Fig. 2 in capacitive operation.

Q_4 are driven with an arbitrary phase difference φ with respect to the voltage source V_s. The switching frequency of Q_1–Q_4 is equal to the frequency of V_s.

Fig. 3 and Fig. 4 show waveforms in the transient and steady states when automatically adjusting the resonance frequency of the resonator which operates as the inductive or capacitive resonator. As shown in Fig. 3 (a) and Fig. 4 (a), the time integrations of the current charging and discharging the C_A are unbalanced in the transient state. As a result, the voltage of C_A increases. Because the capacitance of C_A is sufficiently larger than the C_r, C_A operates as a voltage source and supplies current to the resonator. A part of the current in the resonator generated by C_A operates to cancel the reactive current generated by V_s. In other words, the ATAC injects the reactive current in the resonator. Therefore, the ATAC equivalently adjusts the resonance frequency of the resonator. Then, when the time integration of the current charging the C_A matches the time integration of the current discharging the C_A by adjusting the resonance frequency, it becomes the steady state shown in Fig. 3 (b) and Fig. 4 (b).

As shown in Fig. 3 (b) and Fig. 4 (b), the phase difference between Q_1 (and Q_4) and I_L is always π or $3\pi/2$ in the steady state. Therefore, the phase of the resonant current can be arbitrarily adjusted by changing φ. Especially, in case of Fig. 3, when φ is set to $3\pi/2$, the reactive current generated by V_s can be canceled completely. Therefore, the resonator operates purely as resistive circuit. On the other hand, in case of Fig. 4, when φ is set to $\pi/2$, the reactance of the resonator can be equivalently canceled completely.

In case of the inductive operation (Fig. 3), the ATAC does not operate unless the phase difference φ is set to $\pi<\varphi<2\pi$ because it is necessary for C_A to generate a negative voltage in order for the ATAC to operate at $0<\varphi<\pi$. However, because Q_1–Q_4 have antiparallel diodes, negative voltage is not generated in C_A. For the same reason, in case of the capacitive operation (Fig. 5), the ATAC does not operate unless the phase difference φ is set to $0<\varphi<\pi$.

Moreover, in case of the inductive operation (Fig. 4), Q_1–Q_4 can achieve the ZVS turn-on. On the other hand, in the case of the capacitive operation (Fig. 5), Q_1–Q_4 operate hard switching. Therefore, compensating the inductive resonator is more efficient than compensating the capacitive resonator.

III. Theoretical Analysis

In this section, the RIC-WPT with repeater applying the ATAC is analyzed. In order to compare the robustness of the repeater of the both case wherein the ATAC is applied to the RIC-WPT system or does not, we derive the induced current in the repeater and the current in the transmitter. First, we analyze the RIC-WPT system to which the ATAC is not applied. Then, we suggest the method which can improve the robustness of the repeater using the ATAC.

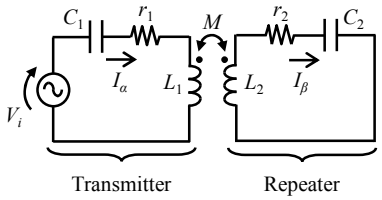

Fig. 5. Simplified equivalent circuit of Fig. 1.

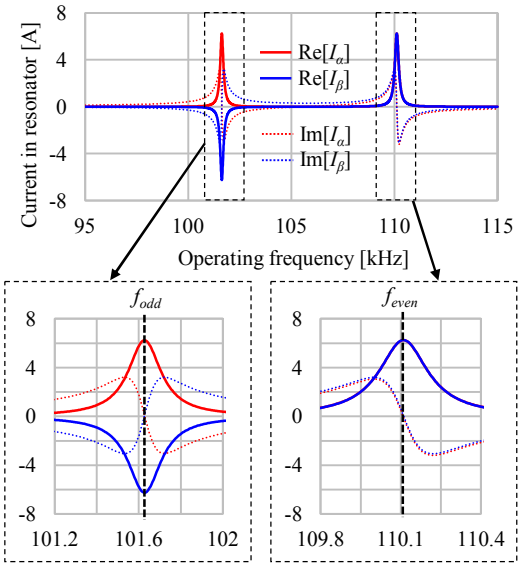

Fig. 6. Real and imaginary parts of current of fig. 5.

A. RIC-WPT without ATAC

Firstly, Fig. 5 illustrates the simplified equivalent circuit of Fig. 1, where L_1 and L_2 are the self-inductance of W_1 and W_2, C_1 and C_2 are the capacitance of the resonance capacitor, r_1 and r_2 are the series parasitic resistance of the transmitter and the repeater, and M is mutual inductance between W_1 and W_2.

In this study, we target the RIC-WPT system for small-sized low-power applications such as small mobile devices and implanted biomedical devices. In general, in case of these applications, the receiving coil has the relatively small magnetic coupling to the other coils [18]. Hence, for the simplification, it is assumed that the influence of the receiving resonator is ignored. The RIC-WPT systems which are easily affected by the receiving resonator will be addressed in other future paper.

In addition, for convenience, we assume that the transmitter and repeater have the same parameter, i.e. $L_1=L_2=L$, $C_1=C_2=C$, $r_1=r_2=r$.

According to the Kirchhoff's voltage law, the system of Fig. 5 can be described as

$$\begin{cases} V_i=rI_\alpha+j(\omega L-1/\omega C)I_\alpha-j\omega MI_\beta, \\ -j\omega LI_\beta+j\omega MI_\alpha=rI_\beta-jI_\beta/\omega C. \end{cases} \quad (1)$$

Then, we define the impedance as

$$j(\omega L-1/\omega C)=jX. \quad (2)$$

By substituting (2) into (1), the currents of the transmitter and the repeater can be derived accordingly as

$$I_\alpha=V_i(N_{1R}+jN_{1I})/D_p, \quad (3)$$

$$I_\beta=V_i(N_{2R}+jN_{2I})/D_p, \quad (4)$$

where, N_{1R}, N_{1I}, N_{2R}, N_{2I}, and D_p are defined as

$$\begin{aligned} N_{1R}&=r\{(r^2+X^2)+\omega^2M^2\},\\ N_{1I}&=X(\omega^2M^2-r^2-X^2),\\ N_{2R}&=2\omega MrX,\\ N_{2I}&=\omega M(\omega^2M^2+r^2-X^2),\\ D_p&=2\omega^2M^2\{r^2-X^2+\omega^2M^2/2\}+(r^2+X^2)^2. \end{aligned} \tag{5}$$

Next, we discuss the method which can improve the robustness of the induced current in repeater by applying the ATAC to Fig. 5. From (3), (4), and (5), the real and imaginary parts of the current in each resonator can be described as shown in Fig. 6, where f_{odd} and f_{even} are the odd and even mode resonance frequencies, respectively. Parameters V_i, L, M, C, and r are set at 2.25V, 140.70μH, 11.26μH, 16.14nF, and 0.18Ω, respectively.

As shown in Fig. 6, Re[I_α] and Re[I_β] are in opposite phases at f_{odd}. Furthermore, the magnitude of Im[I_α] and Im[I_β] are almost zero. On the other hand, at f_{even}, Re[I_α] and Re[I_β] are in phases and Im[I_α] and Im[I_β] are almost zero.

Therefore, if the ATAC is operated to cancel the Im[I_α] or Im[I_β], it may be possible to drive equivalently the RIC-WPT as either of two resonance modes even if the operating frequency deviates from the frequency corresponding to the resonance mode. Therefore, we propose Fig. 7 which the ATAC is applied to the repeating side in order to cancel Im[I_β] and Fig. 8 which the ATAC is applied to the transmitting side in order to cancel Im[I_α]. Next, we analyze Fig. 7 and Fig. 8.

B. RIC-WPT with ATAC of Repeating Side (Fig. 7)

In order to derive I_{L1} and I_{L2}, we derive V_A in the steady state, where V_A is the effective value of the fundamental wave component of the rectangular wave voltage generated by the ATAC.

The phase diagram of Fig. 9 shows V_i and V_A of Fig.7. Because the phase of Q_1 and Q_4 is advanced by φ with respect to V_i, the phase difference between V_A and V_i is φ. To simplify the analysis, the phasor diagram with V_i as a reference shown in Fig. 9 (a) is rotated clockwise by $\varphi-\pi/2$. As a result, the phasor diagram with jV_A as a reference shown in Fig. 9 (b) is obtained.

I'_α, I'_β are defined as I_α and I_β after rotating the phasor diagram, respectively. From (3), I'_α and I'_β in the phasor diagram of Fig. 9 (b) can be expressed as

$$\begin{aligned} \mathrm{Re}[I'_\alpha]&=V_i(N_{1R}\sin\varphi+N_{1I}\cos\varphi)/D_p,\\ \mathrm{Im}[I'_\alpha]&=V_i(-N_{1R}\cos\varphi+N_{1I}\sin\varphi)/D_p,\\ \mathrm{Re}[I'_\beta]&=V_i(N_{2R}\sin\varphi+N_{2I}\cos\varphi)/D_p,\\ \mathrm{Im}[I'_\beta]&=V_i(-N_{2R}\cos\varphi+N_{2I}\sin\varphi)/D_p. \end{aligned} \tag{6}$$

In the steady state, the imaginary part of I_{L2} in Fig. 9 (b) is zero because the imaginary part of the currents generated by V_A and V_i cancel each other. Therefore, Im[I_{L2}] expressed as

$$\mathrm{Im}[I_{L2}]=\mathrm{Im}[I'_\beta]+\mathrm{Im}[-jV_A/Z_o]=0, \tag{7}$$

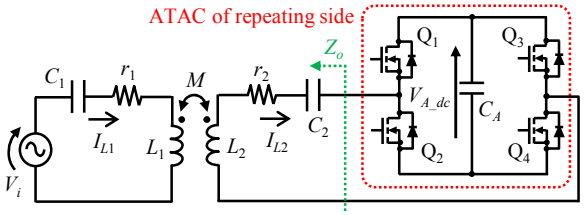

Fig. 7. RIC-WPT with ATAC of repeating side.

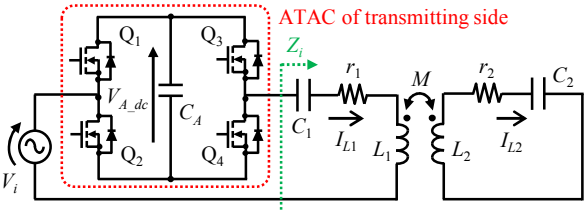

Fig. 8. RIC-WPT with ATAC of transmitting side.

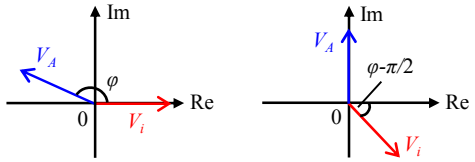

(a) Reference is Vi (b) Reference is jV_A

Fig. 9. Phasor Diagram of Fig. 7 and Fig. 8.

where, Z_o expressed as

$$Z_o=r\left(1+\frac{\omega^2M^2}{r^2+X^2}\right)+jX\left(1-\frac{\omega^2M^2}{r^2+X^2}\right). \tag{8}$$

By substituting (6) and (8) into (7), V_A can be derived accordingly as

$$V_A=2\sqrt{2}V_{A\_dc}/\pi=V_i(-N_{2R}\cos\varphi+N_{2I}\sin\varphi)/N_{1R}. \tag{9}$$

I_{L2} is represented by the superposition of the current by V_A and the current by V_i. Therefore, I_{L2} expressed as

$$\begin{aligned} I_{L2}&=\mathrm{Re}[I'_\beta]+\mathrm{Re}[-jV_A/Z_o]\\ &=\{(N_{2R}\sin\varphi+N_{2I}\cos\varphi)V_i+N_{1I}V_A\}/D_p. \end{aligned} \tag{10}$$

Then, we derive I_{L1}. Similar to equation (10), I_{L1} is also represented by the superposition of the currents generated by V_i and V_A. The real and imaginary parts of I_{L1} generated by V_i are expressed by (6). Moreover, the real and imaginary parts of I_{L1} generated by V_A can be derived using the Kirchhoff's voltage law similar to (3) and (4). Therefore, I_{L1} can be expressed as

$$I_{L1}=\sqrt{\left(\mathrm{Re}[I'_\alpha]+\frac{N_{2I}}{D_p}V_A\right)^2+\left(\mathrm{Im}[I'_\alpha]-\frac{N_{2R}}{D_p}V_A\right)^2}. \tag{11}$$

C. RIC-WPT with ATAC of Transmitting Side (Fig. 8)

In case of Fig. 8, in order to derive I_{L1} and I_{L2}, we also derive V_A similar to the case of Fig. 7. Fig.9 (b) is used for the phasor diagram for analyzing Fig. 8.

In the steady state, the imaginary part of I_{L1} equal to zero because the phase difference between V_A and I_{L1} is always π or 3π/2 as explained in previous section. Therefore, Im[I_{L1}] can be described as

$$\mathrm{Im}[I_{L1}]=\mathrm{Im}[I'_{\alpha}]+\mathrm{Im}[-jV_A/Z_i]=0\,, \tag{12}$$

where, Z_i expressed as

$$Z_i=Z_o=r\left(1+\frac{\omega^2M^2}{r^2+X^2}\right)+jX\left(1-\frac{\omega^2M^2}{r^2+X^2}\right). \tag{13}$$

By substituting (6) and (13) into (12), V_A can be derived accordingly as

$$V_A=2\sqrt{2}V_{A\_dc}/\pi=V_i(-N_{1R}\cos\varphi+N_{1I}\sin\varphi)/N_{1R}. \tag{14}$$

I_{L1} is represented by the superposition of the current by V_A and the current by V_i. Therefore, I_{L1} expressed as

$$\begin{aligned} I_{L1}&=\mathrm{Re}[I'_{\alpha}]+\mathrm{Re}[-jV_A/Z_i]\\ &=\{(N_{1R}\sin\varphi+N_{1I}\cos\varphi)V_i+N_{1I}V_A\}/D_p\,. \end{aligned} \tag{15}$$

Finally, similar to (11), I_{L2} is obtained as

$$I_{L2}=\sqrt{\left(\mathrm{Re}[I'_{\beta}]+\frac{N_{2I}}{D_p}V_A\right)^2+\left(\mathrm{Im}[I'_{\beta}]-\frac{N_{2R}}{D_p}V_A\right)^2}\,. \tag{16}$$

IV. Discussion and Experimental Results

Based on the analysis in the previous section, we evaluate the effectiveness of the proposed systems (Fig. 7 and Fig. 8) when the frequency splitting phenomenon occurs. In addition, we confirm the appropriateness of the analysis results of the previous section by experiment and simulation.

Table I shows the circuit parameters for the experiment and simulation. Fig. 10 shows the photographs of experimental setup of the RIC-WPT system with the ATAC of the repeating side. In the experiment, V_i of Fig. 5, Fig. 7, and Fig. 8 are generated by the half-bridge inverter. The gate signals for the ATAC of Fig. 7 and Fig. 8 are generated using the function generator. Moreover, as pointed out in the previous section, the phase difference φ is set to $\pi/2$ or $3\pi/2$ in order to cancel $\mathrm{Im}[I_\alpha]$ or $\mathrm{Im}[I_\beta]$.

Then, we define frequency regions as shown in Fig. 11, where f_0 is natural resonance frequency of the transmitter and the repeater. As pointed out in Section II, negative voltage cannot be generated in C_A of the ATAC because Q_1–Q_4 have antiparallel diode respectively. Therefore, φ is selected as $\pi/2$ or $3\pi/2$ so that V_{A_dc} does not become negative. Specifically, in the case of the RIC-WPT with the ATAC of the repeating side (Fig .7), φ is set to $\pi/2$ in the frequency regions II and III, and φ is set to $3\pi/2$ in the frequency regions I and IV. On the other hand, in the case of the RIC-WPT with the ATAC of the transmitting side

TABLE I
Circuit Parameters for Experiment and Simulation

Input AC voltage	V_i	1.80V
Self-inductance of W_1	L_1	55.35μH
Parasitic resistance of W_1	r_1	0.16Ω
Capacitance of transmitter	C_1	12.15nF
Self-inductance of W_2	L_2	55.59μH
Parasitic resistance of W_2	r_2	0.16Ω
Capacitance of repeater	C_2	12.13nF
Mutual inductance	M	5.55μH
Phase difference	φ	$\pi/2$ or $3\pi/2$

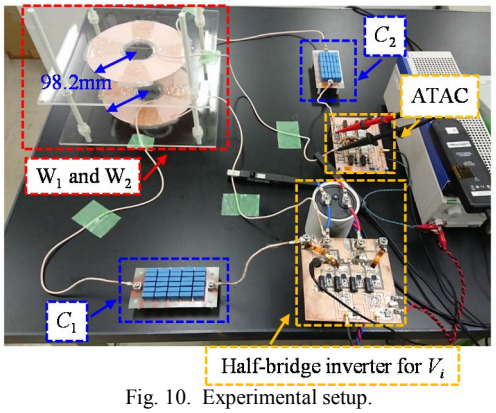

Fig. 10. Experimental setup.

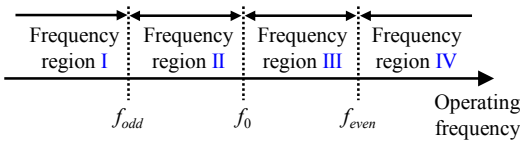

Fig. 11. Definition of frequency regions.

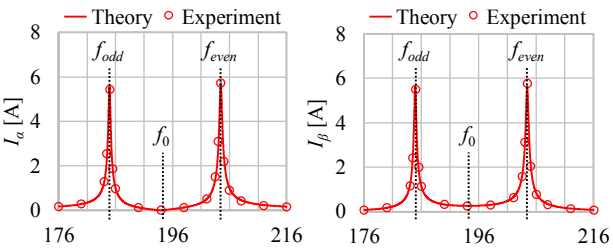

(a) Current in transmitter (b) Current in repeater
Fig. 12. Calculated and experimental results of frequency characteristics.

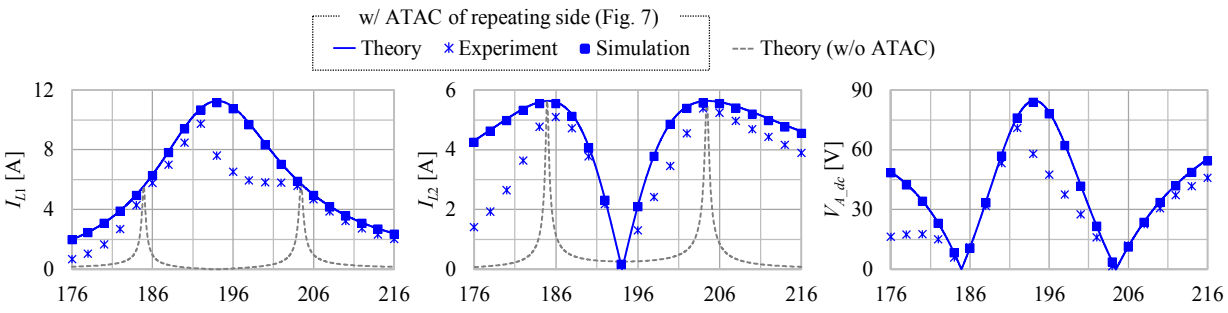

(a) Current in transmitter (b) Current in repeater (c)Voltage of ATAC
Fig. 13. Calculated, simulated, and experimental results of frequency characteristics for the RIC-WPT which applied ATAC to repeating side.

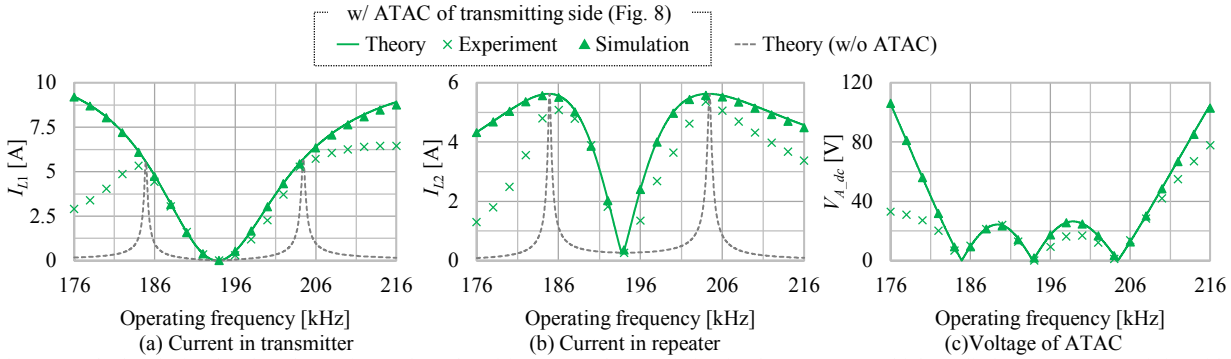

(a) Current in transmitter (b) Current in repeater (c)Voltage of ATAC

Fig. 14. Calculated, simulated, and experimental results of frequency characteristics for the RIC-WPT which applied ATAC to transmitting side.

(Fig. 8), φ is set to $\pi/2$ in the frequency regions I and III, and φ is set to $3\pi/2$ in the frequency regions II and IV.

In order to confirm the appropriateness of the analysis results of the previous section, we evaluate the frequency characteristic of Fig. 5, Fig. 7, and Fig. 8. Firstly, Fig. 12 shows the calculated and experimental results of the frequency response of the current in each resonator. As can be seen form Fig. 12, the experimental results correspond well with the calculated values in case of the RIC-WPT system without the ATAC.

Then, calculated, simulation and experimental results of the frequency characteristics of the RIC-WPT which the ATAC is applied to the repeating side (Fig. 7) and the RIC-WPT which the ATAC is applied to the transmitting side (Fig.8) are shown in Fig. 13 and Fig. 14, respectively. In cases of the RIC-WPT with the ATAC, the experimental results have some error with respect to the calculated value compared with the RIC-WPT without the ATAC. These errors occurred because the Q-factor of the resonator used in the experiment is as large as about several hundreds, so that the slight conduction loss and switching loss of Q_1–Q_4 in the ATAC are relatively easily influence to experimental results. In fact, the simulation results that the conduction and switching losses are not included are corresponded well with the calculated values. Therefore, the appropriateness of the theoretical analysis in the previous section can be confirmed.

As can be seen Fig. 13 and Fig. 14, the error is particularly large in the frequency regions I and III because the switches (Q_1–Q_4) of the ATAC cannot be realized ZVS (Zero Voltage Switching) turn-on in these frequency regions as shown in Table II, where HS represents Hard Switching. Therefore, when the ATAC is applied to the RIC-WPT, it is desirable to apply it to the frequency range which ZVS turn-on can be realized.

TABLE II
SOFT SWITCHING ANALYSIS OF ATAC

Frequency region	I	II	III	IV
Q_1–Q_4 of ATAC (repeating side)	HS turn-on	ZVS turn-on	HS turn-on	ZVS turn-on
Q_1–Q_4 of ATAC (transmitting side)	HS turn-on	ZVS turn-on	HS turn-on	ZVS turn-on

From Fig. 14 (b), the RIC-WPT with the ATAC of the transmitting side can increase I_{L2} in all frequency regions compared to the RIC-WPT without the ATAC. Similarly, as can be seen Fig. 13 (b), the RIC-WPT with the ATAC of the repeating side can increase I_{L2} in a wide frequency range as compared with the RIC-WPT without the ATAC except frequency near f_0. Moreover, in the cases of RIC-WPT systems with the ATAC, the frequency characteristic of I_{L2} can be made gentle near f_{odd} and f_{even} compared to the RIC-WPT without the ATAC. Therefore, I_{L2} can be kept large even at frequencies a little deviated from the frequency at which I_{L2} reaches a peak.

As can be seen from Fig. 13 (b) and Fig. 14 (b), the frequency characteristics of I_{L2} are almost same between the two kinds of the RIC-WPT with the ATAC. On the other hand, the frequency characteristics of I_{L1} and V_{A_dc} are significantly different between the two kinds of the RIC-WPT with ATAC. In the frequency regions I and IV, the RIC-WPT with the ATAC of the repeating side (Fig .7) is superior to the RIC-WPT with the ATAC of the transmitting side (Fig. 8) because I_{L1} and V_{A_dc} can be made

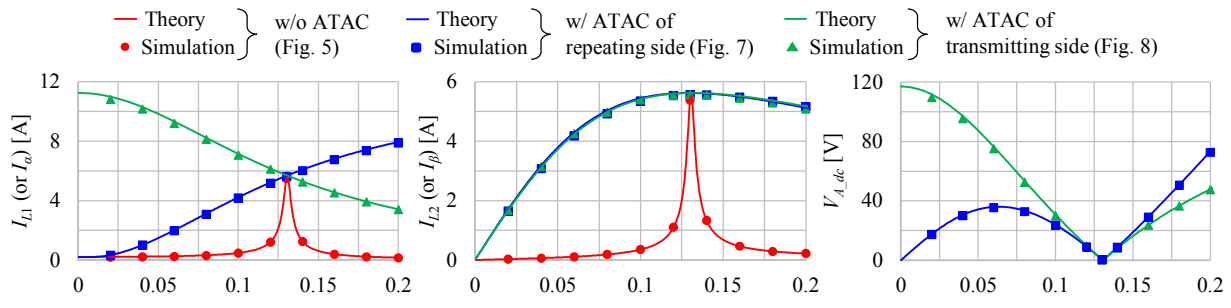

(a) Current in transmitter (b) Current in repeater (c)Voltage of ATAC

Fig. 15. Current in each repeater and voltage of ATAC according to coupling coefficient changing (Operating frequency is set to 208.0kHz).

smaller. Meanwhile, in the frequency regions II and III, the RIC-WPT with the ATAC of the transmitting side (Fig. 8) is more advantageous than the RIC-WPT with the ATAC of the repeating side (Fig .7).

Next, under the operating frequency is arbitrarily fixed, we evaluate the characteristics when the coupling coefficient k is changed, where k is defined as $k=M/L$. The operating frequency is set to 208.0 kHz. Fig. 15 shows the evaluation results. From Fig. 15, when the ATAC is not applied, a large current cannot be induced to the repeater unless the coupling coefficient is set to a specific value. This means that the robustness of the repeater against the misalignment is low. On the other hands, when the ATAC is applied, a relatively large current can be induced to the repeater in a wide coupling coefficient range. Therefore, the robustness of the repeater can be improved by applying the ATAC.

V. CONCLUSIONS

The frequency splitting phenomenon easily occurs in the induced current of the repeater because the Q-factor of the repeater is high. Therefore, the repeater has low robustness against misalignment. In order to improve the robustness of the repeater, we applied the ATAC to the RIC-WPT with the repeater. As a result, it is clarified that the induced current in the repeater can be kept large in a relatively wide operating frequency range which is slightly different from the resonance frequency. Moreover, experiment and simulation successfully verified effectiveness of the proposed system as well as appropriateness of the theoretical analysis.

REFERENCES

[1] C.-S. Wang, G. A. Covic, and O. H. Stielau, "Power transfer capability and bifurcation phenomena of loosely coupled inductive power transfer systems," *IEEE Trans. Ind. Electron.*, vol. 51, issue. 1, pp. 148–157, Feb. 2004.

[2] D. H. Tran, V. B. Vu, and W. choi, "Design of a high-efficiency wireless power transfer system with intermediate coils for the on-board chargers of electric vehicles," *IEEE Trans. power. Electron.*, vol. 33, issue. 1, pp. 175–187, Jan. 2018.

[3] D. Ahn and S. Hong, "Wireless power transmission with self-regulated output voltage for biomedical implant," *IEEE Trans. Ind. Electron.* vol. 61, issue. 5, pp. 2225–2235, May. 2014.

[4] D. Ahn, S. Hong, "A study on magnetic field repeater in wireless power transfer," *IEEE Trans. on Industrial Electronics*, vol. 60, no. 1, pp. 360–371, 2013.

[5] K. Lee and S. H. Chae, "Power transfer efficiency analysis of intermediate-resonator for wireless power transfer," *IEEE Trans. power. Electron.*, vol. 33, issue. 3, pp. 2484–2493, Mar. 2018.

[6] P. K. S. Jayathurathnage, and D. M. Vilathgamuwa, "Optimization of a wireless power transfer system with a repeater against load variations," *IEEE Trans. Ind. Electron.*, vol. 64, issue. 10, pp. 7800–7809, Oct. 2017.

[7] W. Q. Niu, J. X. Chu, W. Gu, and A. D. Shen, "Exact analysis of frequency splitting phenomena of contactless power transfer systems," *IEEE Trans. on Circuit and Systems*, vol.60, no. 6, pp. 1670–1677, Jun. 2013.

[8] R. Huang, B. Zhang, D. Qiu, and Y. Zhang, "Frequency splitting phenomena of magnetic resonant coupling wireless power transfer," *IEEE Trans. on Magnetics*, vol. 50, no. 11, 8600204, Nov. 2014.

[9] D. -W. Seo, J. -H. Lee, and H. -S. Lee, "Optimal coupling to achieve maximum output power in a WPT system," *IEEE Trans. power. Electron.*, vol. 31, issue. 6, pp. 3994–3998, Jun. 2016.

[10] O. Karaca, F. Kappeler, D. Waldau, R. M. Kennel, and J. Rackles, "Eigenmode analysis of a multiresonant wireless energy transfer system," *IEEE Trans. Ind. Electron.*, vol. 61, issue. 8, pp. 4134–4141, Aug. 2014.

[11] D. -W. Seo and J. -H. Lee, "Frequency-tuning method using the reflection coefficient in a wireless power transfer system," *IEEE Microw. Compon. Lett.*, vol. 27, issue. 11, pp. 959–961, Nov. 2017.

[12] Y. Li, C. Zhang, Q. Yang, J. Li, Y. Zhang, X. Zhang, and M. Xue, "Improved ant colony algorithm for adaptive frequency-tracking control in WPT system," *IET Microw. Antennas Propag*, vol. 12, issue. 1, pp. 23–28, Jan. 2018.

[13] R. Mai, P. Yue, Y. Liu, Y. Zhang, and Z. He, "A dynamic tuning method utilizing inductor paralleled with load for inductive power transfer," *IEEE Trans. power. Electron.*, to be published.

[14] A. Trigui, S. Hached, F. Mounaim, A. C. Ammari, and M. Sawan, "Inductive power transfer system with self-calibrated primary resonant frequency," *IEEE Trans. on Power Electronics*, vol. 30, no. 11, pp. 6078–6087, Nov. 2015.

[15] N. Liu, and T. G. Habetler, "An active-rectifier-based maximum efficiency tracking method using an additional measurement coil for wireless power transfer," *IEEE Trans. Power Electron.*, vol. 33, issue. 1, pp. 716–728, Jan. 2018.

[16] T. Isobe, K. Kobayashi, K. Wakasugi, and R. Shimada, "Efficiency improvement of contactless energy transfer systems using series compensation device named MERS," in *Proc. 14th European Conf. Power Electron. Applicat. (EPE)*, 2011, Birmingham, pp. 1–10.

[17] Y. Endo and Y. Furukawa, "Proposal for a new resonance adjustment method in magnetically coupled resonance type wireless power transmission," in *Proc. 2012 IEEE MTT-S International Microwave Workshop Series on Innovative Wireless Power Transmission: Technologies, Systems, and Applications (IMWS-IWPT)*, 2012, Kyoto, pp. 263–266.

[18] S. Mao, J. Zhang, K. Song, G. Wei, and C. Zhu, "Wireless power transfer using a field-enhancing coil and a small-sized receiver with low coupling coefficient," *IET power electron.*, vol. 9, issue. 7, pp. 1546–1552, Jun. 2016.